Available online at www.sciencedirect.com
ScienceDirect
International Journal of Heat and Mass Transfer 51 (2008) 2930–2939
International Journal of HEAT and MASS TRANSFER
www.elsevier.com/locate/ijhmt

Convective heat transfer to water near the critical region in a horizontal square duct

Sang-Ho Lee *

Department of Mechanical Engineering, Wonkwang University, Cheonbuk 570-749, Republic of Korea

Received 4 April 2007; received in revised form 10 September 2007
Available online 5 November 2007

Abstract

Numerical analysis has been carried out to investigate forced convective heat transfer to water near the critical region in a horizontal square duct. Near the critical point convective heat transfer in the duct is strongly coupled with large variation of thermophysical properties such as density and specific heat. Buoyancy force parameter has also severe variation with fluid temperature and pressure in the duct. There is flow acceleration along the horizontal duct resulted from fluid density decrease due to the heat transfer from the wall. Local heat transfer coefficient has large variation along the inner surface of the duct section and it depends on pressure. Nusselt number on the center of the bottom surface also has a peak where bulk fluid temperature is higher than the pseudocritical temperature and the peak decreases with the increase of pressure. Flow characteristics of velocity, temperature, and local heat transfer coefficient with water properties are presented and analyzed. Nusselt number distributions are also compared with other correlations for various pressures in the duct.

Keywords: Critical region; Convective heat transfer; Horizontal square duct; Pseudocritical temperature; Thermophysical properties; Buoyancy force

1. Introduction

Recently fluids near the critical region have been used widely in many application areas. Especially heat exchanger systems of power generation, superconductor, and environmental systems for fluids near the critical region are of continuing interest. Near the thermodynamic critical point fluid flow and heat transfer characteristics are quite different from those of constant property case and they are very complicated due to the large variation of thermodynamic and transport properties as shown in Fig. 1. The characteristics of momentum and heat transfer to the supercritical fluid are strongly coupled with the highly non-linear variation of the fluid properties, which makes flow phenomena more unpredictable compared with the constant property case.

Since 1930s many experimental and theoretical studies [1–16] have been performed to investigate the fluid flow and heat transfer phenomena near the critical point due to various applications. Most of these studies are for convective heat transfer in a tube under steady state which is typical of various applications, and a lot of heat transfer correlations [1,2,25] have been suggested. For convective heat transfer near the critical region in non-circular ducts less research has been done relatively although application areas are increasing. Pioro et al. [1,13] analyzed heat transfer correlations and experimental data on heat transfer to supercritical fluids inside channels through the literature survey. They showed that there is a significant difference in heat transfer coefficients calculated from various correlations and the differences in the prediction of supercritical heat transfer are due to the significant variations in thermophysical properties near the pseudocritical temperatures. Lee and Howell [5,6] investigated turbulent convective heat transfer in a vertical tube with numerical modeling which includes the effects of fluid property variations near the

* Tel.: +82 63 850 6687; fax: +82 63 850 6691.
E-mail address: lsheagle@wonkwang.ac.kr

0017-9310/$ - see front matter © 2007 Elsevier Ltd. All rights reserved.
doi:10.1016/j.ijheatmasstransfer.2007.09.016

Nomenclature

b	internal duct width (m)
D_h	hydraulic diameter (m)
C_p	specific heat at constant pressure (J/kg K)
Gr	Grashof number, $\rho^2 g\beta q_w D^4/(16k\mu^2)$
Gr^*	local Grashof number, $\lvert\rho_w - \rho_b\rvert\rho_b g D_h^3/\mu_b^2$
h	heat transfer coefficient (W/m^2 K)
i	enthalpy (J/kg)
Nu	Nusselt number, hD/k_b
P	pressure (Pa)
P_R	reduced pressure, P/P_c
q	heat flux (W/m^2)
Re_{in}	inlet Reynolds number
s	circumferential distance inside the duct (m)
T	temperature (K)
T^*	non-dimensional temperature, $k_{in}(T - T_{in})/q_w \cdot D_h$
T_{pc}	pseudocritical temperature (K)
u	velocity (m/s)
κ	turbulent kinetic energy (m^2/s^2)
ε	dissipation rate (m^2/s^3)
μ_t	turbulent viscosity (kg/m s)
ρ	density (kg/m^3)

Subscripts

c	critical point
b	bulk fluid
i, j	general spatial indices
in	inlet
w	wall

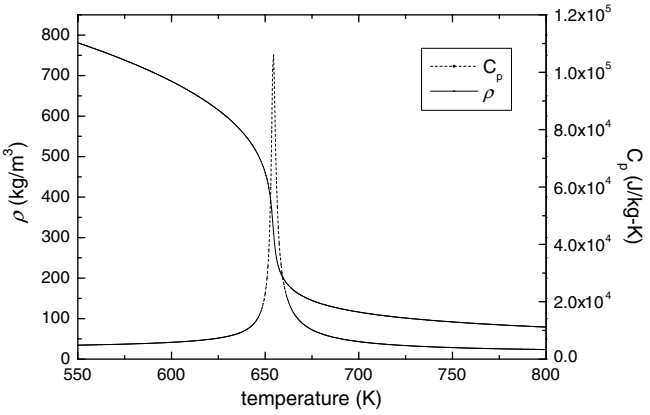

Fig. 1. Thermophysical properties variation of water near the critical region ($P = 24$ MPa).

critical point. Liao and Zhao [10,11,26] experimentally analyzed heat transfer for supercritical carbon dioxide flowing in micro channels with numerical simulation, and suggested a heat transfer correlation from the experimental results.

Asinari [14] also numerically investigated turbulent convective heat transfer in micro channel for supercritical CO_2. He proposed a modified turbulence closure model with velocity fluctuations and thermophysical properties variation within the frame work of mixing length theory and showed from comparison with other correlations that heat transfer impairment exists in the micro channels. Tatsumoto et al. [15] performed numerical investigation on the heat transfer characteristics in a two-dimensional parallel duct for various gaps with helium and showed that steady-state critical heat flux increases with the increase of gap distance. McEligot and Jackson [16] analyzed deterioration criteria for convective heat transfer in non-circular duct using typical flow parameters such as fluid properties variation, acceleration, and buoyancy force. Pitla et al. [24] suggested a correlation to predict heat transfer coefficient of supercritical carbon dioxide during in-tube cooling based on the numerical predictions and experimental data. Zhou and Krishnan [27] predicted laminar and turbulent heat transfer for channel flow of supercritical CO_2 and showed that heat transfer rate for upward flow could be less than no-gravity case because of lower turbulent viscosity. And Hirota et al. [17] performed an experimental analysis of turbulent heat transfer in a straight square duct for air. Yucel and Guven [18], and Da Silva Miranda and Anand [20] investigated convective heat transfer enhancement characteristics in channels with porous material, and Luo et al. [19] also numerically predicted forced convection of a fully developed turbulent flow in parallel plates with periodic ribs.

These studies show that the properties variation of supercritical fluids severely affect fluid flow and heat transfer and they should not be neglected near the critical region. Despite the several studies convective heat transfer characteristics in a non-circular duct for the supercritical fluids are not well understood while there is not sufficient experimental data to analyze because of the large number of flow variables and difficult range of thermodynamic pressure and temperature. In this study forced convective heat transfer to water near the critical region inside a horizontal square duct is predicted by numerical modeling to investigate the momentum and heat transfer coupled with the large variations of thermodynamic and transport properties including proximity effect to the critical point.

2. Numerical modeling

The problem to be analyzed is turbulent forced convective heat transfer to near-critical water flowing through a smooth-walled horizontal square duct with constant heat

flux. The flow is assumed to be steady-state with local thermodynamic equilibrium. The time-averaged three-dimensional governing equations of continuity, momentum, and energy with standard approximations and turbulence modeling are as follows:

(a) Continuity

$$\frac{\partial}{\partial x_i}(\rho u_i) = 0 \tag{1}$$

(b) Momentum

$$\frac{\partial}{\partial x_j}(\rho u_i u_j) = -\frac{\partial p}{\partial x_j} + \frac{\partial}{\partial x_j}\left(\tau_{ij} + \tau_{ij}^R\right) + \rho g_i \tag{2}$$

(c) Energy

$$\frac{\partial}{\partial x_i}(\rho u_i H) = \frac{\partial}{\partial x_i}\left[\left(\frac{\mu}{Pr} + \frac{\mu_t}{Pr_t}\right)\frac{\partial H}{\partial x_i}\right] + \frac{\partial}{\partial x_i}\left[u_j\left(\tau_{ij} + \tau_{ij}^R\right)\right] - \tau_{ij}^R\frac{\partial u_i}{\partial x_j} - \rho u_i \frac{\partial}{\partial x_i}\left(\frac{u_j u_j}{2}\right) + \rho\varepsilon \tag{3}$$

(d) Turbulent kinetic energy

$$\frac{\partial}{\partial x_i}(\rho u_i k) = \frac{\partial}{\partial x_i}\left[\left(\mu + \frac{\mu_t}{\sigma_k}\right)\frac{\partial k}{\partial x_i}\right] + \tau_{ij}^R\frac{\partial u_i}{\partial x_j} - \rho\varepsilon + \mu_t\left(-\frac{g_i}{\sigma_B\rho}\frac{\partial \rho}{\partial x_i}\right) \tag{4}$$

(e) Dissipation

$$\frac{\partial}{\partial x_i}(\rho u_i \varepsilon) = \frac{\partial}{\partial x_i}\left[\left(\mu + \frac{\mu_t}{\sigma_\varepsilon}\right)\frac{\partial \varepsilon}{\partial x_i}\right] + C_{\varepsilon 1}\frac{\varepsilon}{k}\left[f_1\tau_{ij}^R\frac{\partial u_i}{\partial x_j}\right] + \mu_t C_B\left(-\frac{g_i}{\sigma_B\rho}\frac{\partial \rho}{\partial x_i}\right) - C_{\varepsilon 2}f_2\frac{\rho\varepsilon^2}{k} \tag{5}$$

In this study, the turbulent flow model follows κ–ε model proposed by Lam and Bremhorst [21]. The shear stress tensors have the following forms:

$$\tau_{ij} = \mu\left(\frac{\partial u_i}{\partial x_j} + \frac{\partial u_j}{\partial x_i} - \frac{2}{3}\delta_{ij}\frac{\partial u_k}{\partial x_k}\right) \tag{6}$$

$$\tau_{ij}^R = \mu_t\left(\frac{\partial u_i}{\partial x_j} + \frac{\partial u_j}{\partial x_i} - \frac{2}{3}\delta_{ij}\frac{\partial u_k}{\partial x_k}\right) - \frac{2}{3}\rho k\delta_{ij} \tag{7}$$

Here turbulent viscosity is defined as follows:

$$\mu_t = f_\mu\frac{C_\mu\rho k^2}{\varepsilon} \tag{8}$$

where $f_\mu = [1 - \exp(-0.025R_y)](1 + \frac{20.5}{R_T})^2$, $R_T = \frac{\rho k^2}{\mu\varepsilon}$, $R_y = \frac{\rho\sqrt{k}y}{\mu}$, $f_1 = 1 + (\frac{0.05}{f_\mu})^3$, $f_2 = 1 - \exp(-R_T^2)$.

Constants in the turbulence modeling are defined in Table 1. Pr_t is the turbulent Prandtl number and is set to be 0.9.

As flow boundary conditions fully developed velocity and constant temperature are assumed at the inlet of the duct. The turbulence intensity at the inlet is equal to 5% and the length scale is set to be $0.035D_h$ as in Li et al. [4]. Constant heat flux boundary condition is applied at the duct outside. This numerical analysis is performed on the left half of the parallel duct system with symmetry condition at the vertical section plane. All thermodynamic and transport properties of water are calculated with the computer code of Lester et al. [22]. The geometry is horizontal square duct of stainless steel with length of 1.0 m, inner width of 0.01 m, and thickness of 0.001 m.

Table 1
Constants in the κ–ε model

C_μ	$C_{\varepsilon 1}$	$C_{\varepsilon 2}$	σ_ε	σ_k	σ_B
0.09	1.44	1.92	1.3	1.0	1.0

The governing equations are solved by CFD solver, EFD-Lab with the SIMPLE algorithm [23] using the second order upwind scheme. Convergence is checked by computing the normalized mass residual in the equation of continuity until the residual is less than 10^{-3}. Successive iteration continues until further repetitions cease to produce relative change less than 10^{-3} in the values of each variable. For numerical calculation, orthogonal non-uniform grid system is used to give enough grid points near the wall where there is large variation in heat transfer. Most calculations are based on the grid system of 408,000 and grid dependence was checked with denser grid systems. The differences between the calculated results of temperature and heat transfer coefficient and those with finer grid systems of 650,000 and 815,000 are less than 1%.

3. Results and discussion

3.1. Flow field and thermophysical properties distribution with buoyancy force

Figs. 2–5 show the developing axial velocity and temperature distributions with water properties in the duct for the pressures of $P_R = 1.09$ and 1.36. It can be seen that there is flow acceleration along the duct and it depends on the pressure in the duct. Maximum velocity at $z/b = 80$ for the pressure of $P_R = 1.09$ is increased about 1.7 times higher than that at $z/b = 40$. Flow acceleration is caused by the density decrease due to heat transfer from the wall. As pressure approaches to the critical pressure density variation is more severe and flow acceleration becomes larger. Fluid velocity is high in the upper region near the centerline of the duct due to the buoyancy force. There is very steep temperature gradient close to the top surface and pseudocritical temperature region where there is large variation of specific heat moves downward along the duct. Turbulent viscosity distribution shows that it is quite different from those of density and specific heat. It can be seen that turbulent viscosity is much affected by buoyancy force and steep variation of water properties near the pseudocritical temperature. Its distribution depends on the pressure in the

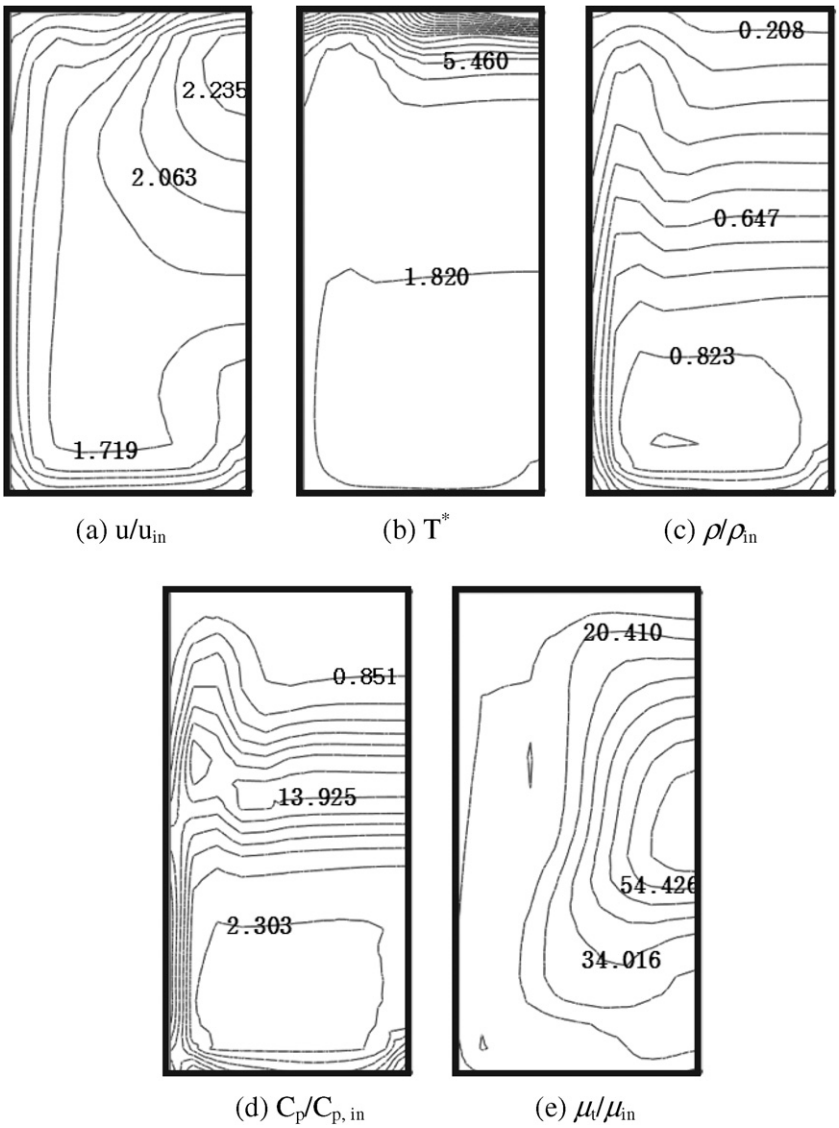

Fig. 2. Axial velocity and temperature distributions with the properties at the section of $z/b = 40$ from the entrance for $P_R = 1.09$, $Re_{in} = 5 \times 10^4$, $q_w = 800\ kW/m^2$, $T_{in} = 620\ K$.

duct and it increases along the duct. It also increases as pressure approaches to the critical pressure and its maximum near the center of the duct section at $z/b = 80$ is increased to more than 2.8 times than that in the duct section at $z/b = 40$. Fig. 6 shows the Grashof number variation with respect to temperature at several pressures for constant heat flux in a duct. As fluid temperature approaches to the pseudocritical temperature the Grashof number increases rapidly and reaches a peak. There is severe variation of the buoyancy force near the pseudocritical temperature, and it becomes even steeper as the pressure approaches to the critical pressure. The peak of the Grashof number at $P_R = 1.09$ is about 3.8 times higher than that at $P_R = 1.36$.

Local buoyancy force based on the density difference between the wall and bulk fluid in the duct can be represented as follows [11]:

$$\frac{Gr^*}{Re^2} = \frac{|\rho_w - \rho_b|\rho_b^2 g u_b D_h^4}{\mu_b^3} \tag{9}$$

This buoyancy force variation with bulk temperature at the center of bottom surface is also shown in Fig. 7. The buoyancy force, Gr^*/Re^2 decreases with the increase of bulk temperature and it depends on the pressure in the duct while it shows transition characteristics between liquid-like and gas-like behavior. As pressure approaches to the critical pressure, the buoyancy force variation becomes steeper near the pseudocritical temperature and T_b/T_{pc} at the steep variation of Gr^*/Re^2 becomes closer to 1. The buoyancy force, Gr^*/Re^2 is much higher than 10^{-3} and it affects the flow field as in Figs. 2–5, especially at the temperature region of $T_b/T_{pc} < 1.01$.

These flow distributions in the duct affect heat transfer characteristics which are quite different from the constant

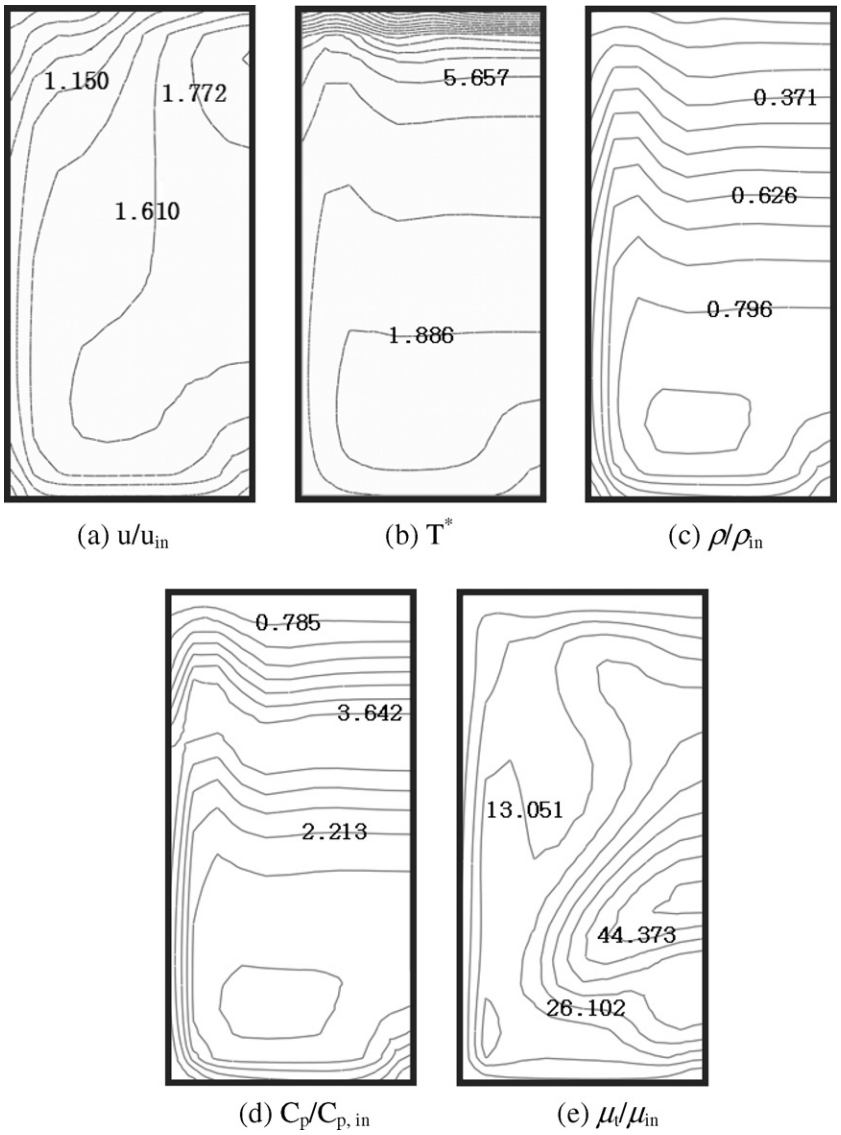

Fig. 3. Axial velocity and temperature distributions with the properties at the section of $z/b = 40$ from the entrance for $P_R = 1.36$, $Re_{in} = 5 \times 10^4$, $q_w = 800\ kW/m^2$, $T_{in} = 620\ K$.

property case [17]. Fig. 8 shows the local heat transfer coefficient distributions inside the surfaces of the duct. Local heat transfer coefficient on the bottom surface is much higher than that on the top surface and the difference depends on the pressure in the duct. As pressure approaches to the critical pressure the difference between the heat transfer coefficients on the bottom and vertical surfaces becomes larger. For $P_R = 1.09$ heat transfer coefficient at the position of $z/b = 40$ is much higher than that at the position of $z/b = 80$, and for $P_R = 1.36$ the difference of the heat transfer coefficients at those positions is relatively reduced. It is due to the improved turbulent transport with high buoyancy force and specific heat, especially close to the pseudocritical temperature where there is very steep variation of density and specific heat as in Figs. 2–5. With heat transfer from the wall water temperature increases and as water temperature approaches to pseudocritical temperature buoyancy force increases very rapidly as in Fig. 6. There is little variation of heat transfer coefficient on the top surface ($0.0 < s/b < 0.5$) with pressure and circumferential distance because of high temperature fluid with gas-like behavior near the surface. With heat transfer from the wall transition behavior from liquid-like phase to gas-like phase of heat transfer coefficient occurs when the fluid passes through pseudocritical temperature region in the duct.

3.2. Heat transfer coefficient distributions along the duct

Fig. 9 shows the heat transfer coefficient distributions at the centers of top and bottom planes along the duct. There is a large difference in the heat transfer coefficient distributions on the top and bottom planes and it depends on the pressure in the duct. It can also be seen that heat transfer

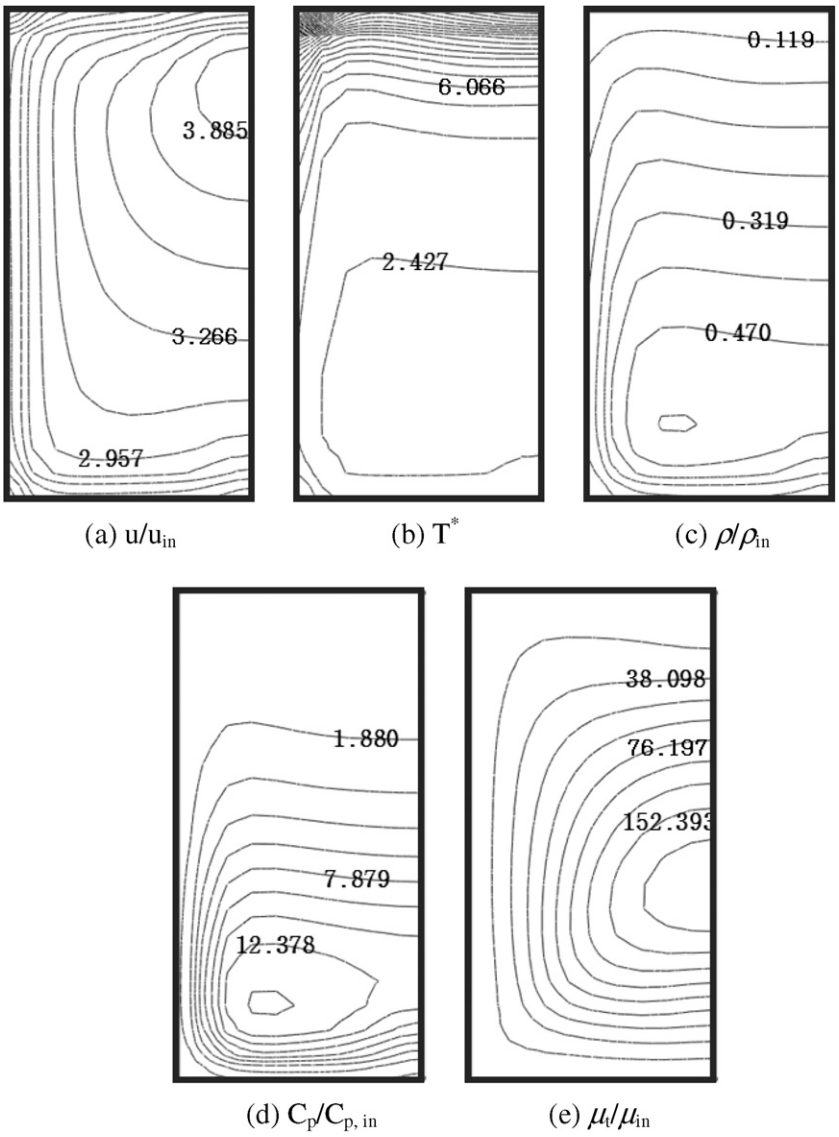

Fig. 4. Axial velocity and temperature distributions with the properties at the section of $z/b = 80$ from the entrance for $P_R = 1.09$, $Re_{in} = 5 \times 10^4$, $q_w = 800\ kW/m^2$, $T_{in} = 620\ K$.

coefficient at the center of top plane decreases near the entrance region and for $z/b > 30$ its variation is little along the duct. It is similar to the no gravity case although there is a little difference near the entrance. However the heat transfer coefficient at the center of the bottom plane increases along the duct. It reaches a peak when the bulk fluid temperature is a little (6.0 K and 9.5 K for $P_R = 1.09$ and $P_R = 1.36$, respectively) higher than pseudocritical temperature, and then decreases. The peak of the heat transfer coefficient increases as pressure approaches to the critical pressure. With the increase of pressure in the duct axial peak position moves to downstream because of pseudocritical temperature increase.

The flow field with properties variation and heat transfer coefficient in the duct affect Nusselt number distribution along the duct. Fig. 10 shows the variation of several Nusselt numbers with bulk fluid enthalpy for various pressures at the center of bottom surface in the duct. These Nusselt numbers are calculated Nu, Nu_{DB} calculated from Dittus–Boelter equation, and Nu_{LZ} which is suggested by Liao and Zhao [11] for horizontal tube flow. Nu_{LZ} includes the buoyancy effect and can be expressed as the following correlation:

$$Nu_{LZ} = 0.124 Re_b^{0.8} Pr_b^{0.4} \left(\frac{Gr^*}{Re_b^2}\right)^{0.203} \left(\frac{\rho_w}{\rho_b}\right)^{0.842} \left(\frac{\overline{C}_p}{C_{p,b}}\right)^{0.384} \tag{10}$$

where the mean specific heat, $\overline{C}_p$ is defined as

$$\overline{C}_p = \frac{i_w - i_b}{T_w - T_b} \tag{11}$$

These Nusselt numbers of Nu, Nu_{DB}, and Nu_{LZ} have quite different behaviors along the duct. Nu increases with bulk enthalpy as in heat transfer coefficient distribution and it reaches a peak when the bulk fluid temperature is

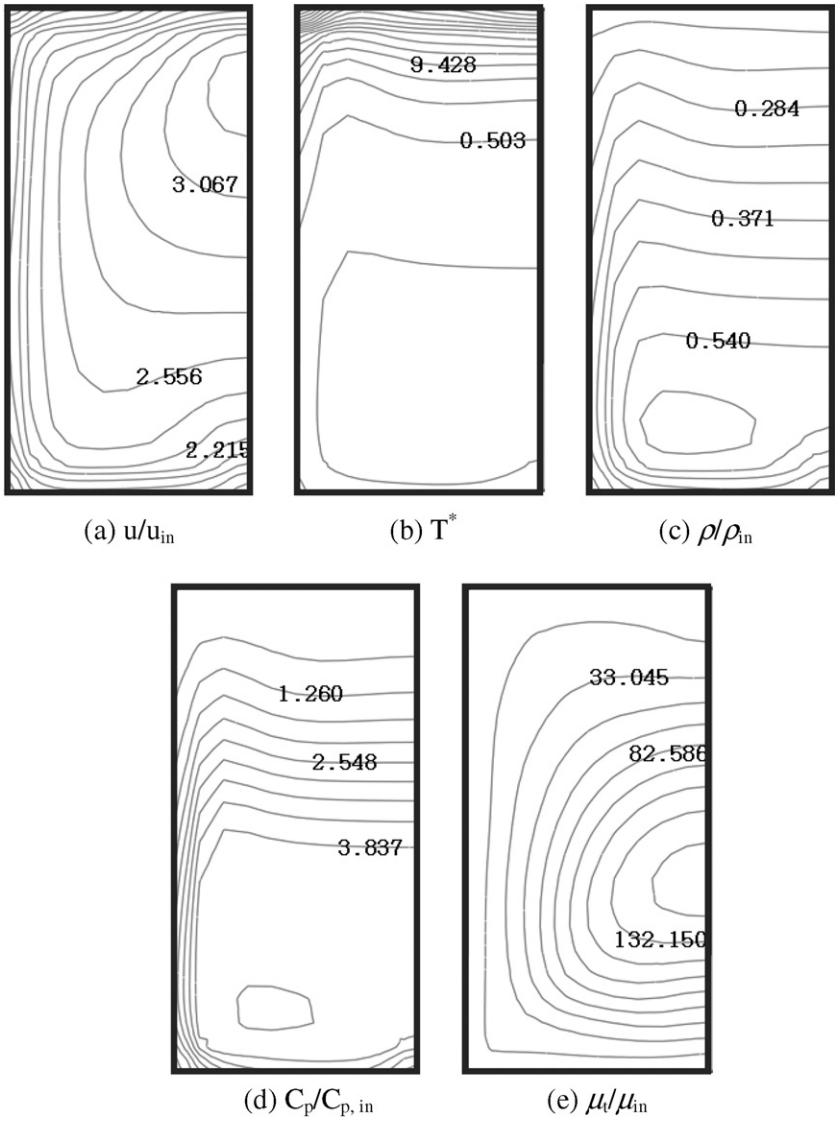

Fig. 5. Axial velocity and temperature distributions with the properties at the section of $z/b = 80$ from the entrance for $P_R = 1.36$, $Re_{in} = 5 \times 10^4$, $q_w = 800\ kW/m^2$, $T_{in} = 620\ K$.

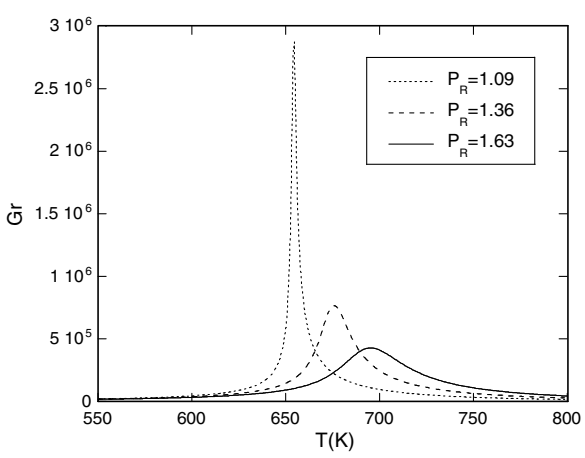

Fig. 6. Grashof number variation with water temperature for various pressures.

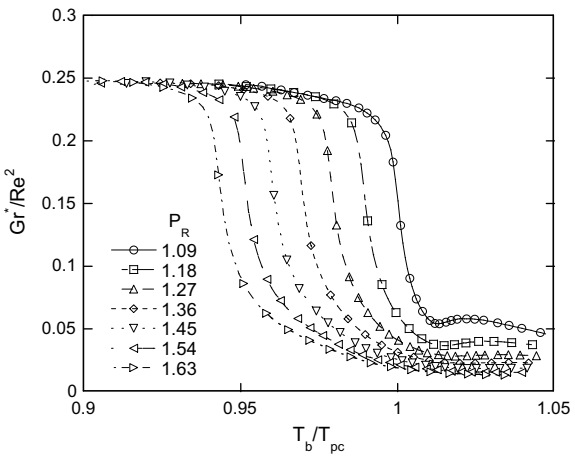

Fig. 7. Local buoyancy force variation with bulk temperature for various pressures at the center of bottom surface.

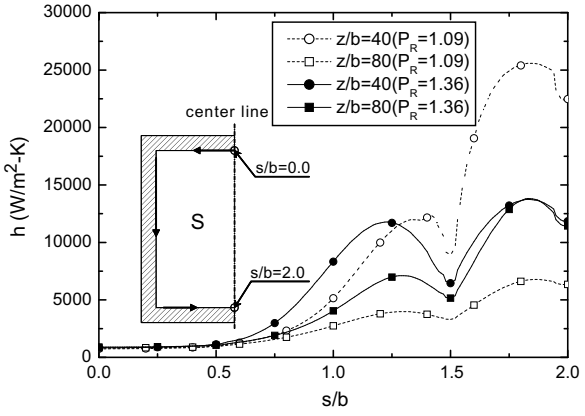

Fig. 8. Local heat transfer coefficient distributions inside the sections of the duct.

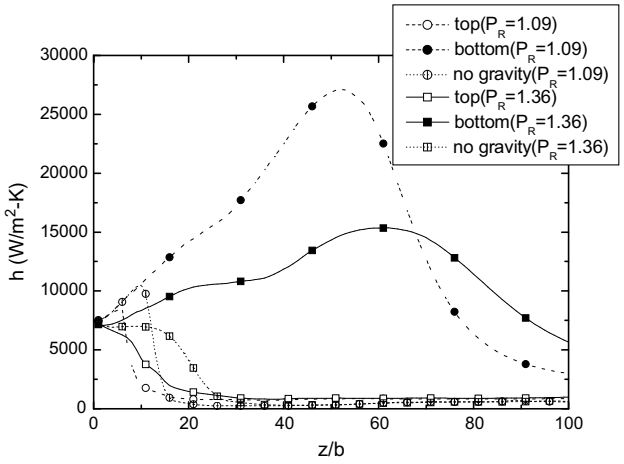

Fig. 9. Local heat transfer coefficient distributions at the centers of top ($s/b = 0.0$) and bottom ($s/b = 2.0$) planes along the duct.

a little (6.0–13.2 K) higher than pseudocritical temperature corresponding to the pressure in the duct and less than wall temperature. And as pressure approaches to the critical pressure the peak of the *Nu* increases very rapidly. Beyond the peak of the *Nu* there is very steep decrease with bulk fluid enthalpy. This increase of *Nu* is also caused by improved turbulent transport due to large turbulent viscosity with high specific heat and buoyancy force as in the heat transfer coefficient. Bulk fluid enthalpy at the peak gradually increases with pressure because of the increase in

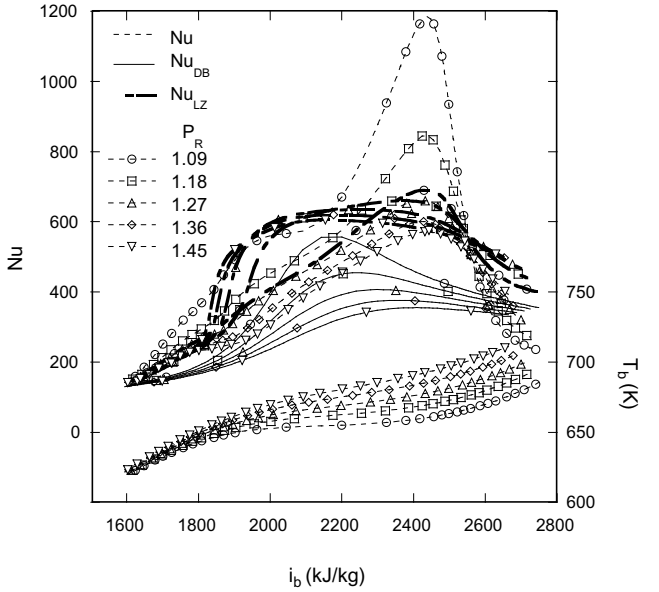

Fig. 10. Comparison of Nusselt number distributions with bulk fluid temperature for various pressures at the centerline of bottom plane in the duct.

pseudocritical temperature. Nu_{DB} also reaches a peak where the bulk fluid temperature is close to the pseudocritical temperature. The peak of Nu_{DB} is much less than that of *Nu* and for $P_R > 1.36$ it is very small. Nu_{LZ} shows intermediate behavior between *Nu* and Nu_{DB}. Nu_{LZ} near the pseudocritical enthalpy is higher than Nu_{DB} and less than *Nu*. Nu_{LZ} also increases near the pseudocritical temperature and it is much higher than Nu_{DB} for overall bulk fluid enthalpy because of large buoyancy force as in Fig. 7. For $P_R < 1.27$ bulk enthalpy at the peak of Nu_{LZ} is much higher than that of Nu_{DB} and close to the bulk enthalpy of *Nu* peak. The difference between *Nu* and Nu_{LZ} increases as pressure approaches to the critical pressure and the maximum difference is about 72% for $P_R = 1.09$ near the peak. Nu_{LZ} has steep variation close to the pseudocritical enthalpy (1800 kJ/kg $< i_b <$ 1900 kJ/kg) for $P_R > 1.09$.

Table 2 shows the variation of bulk fluid temperature at the peak of the Nusselt numbers for various pressures in the duct. As pressure approaches to the critical pressure the differences between the Nusselt numbers increases very severely while bulk fluid temperatures at the peaks become closer to pseudocritical temperature. The ratios of Nu_{peak}/

Table 2
Variation of Nusselt number peaks with bulk fluid temperature in the duct

P_R	Nu_{peak}	$T_b(Nu_{peak})/T_{pc}$	$Nu_{peak}/Nu_{DB,peak}$	$T_b(Nu_{DB,peak})/T_{pc}$	$Nu_{peak}/Nu_{LZ,peak}$	$T_b(Nu_{LZ,peak})/T_{pc}$
1.09	1184.1	1.009	2.128	1.001	1.716	1.009
1.18	845.5	1.011	1.860	1.003	1.282	1.008
1.27	662.0	1.012	1.629	1.005	1.043	1.002
1.36	600.5	1.014	1.596	1.009	0.969	0.998
1.45	570.8	1.015	1.609	1.013	0.943	0.995
1.54	538.8	1.018	1.593	1.017	0.914	0.992
1.63	505.1	1.019	1.554	1.023	0.877	0.992

$Nu_{LZ,peak}$ are about 1.7 and 1.0 for $P_R = 1.09$ and $P_R = 1.36$, respectively, while those of $Nu_{peak}/Nu_{DB,peak}$ are about 2.1 and 1.6. For $P_R > 1.36$ these ratios variation is not so severe. The difference between pseudocritical temperature and bulk fluid temperature at the peak of Nu is higher than those at the peaks of Nu_{LZ} and Nu_{DB} for $P_R < 1.54$. And the difference between the two temperatures increases with the increase of pressure in the duct. For $P_R = 1.09$ $\Delta[T_b(Nu_{peak}) - T_{pc}]$ is about 6.0 K while for $P_R = 1.36$ it is about 9.5 K.

4. Conclusions

Numerical simulations are performed for turbulent forced convective heat transfer in a horizontal heated square duct near the critical point for water. Coupled fluid flow and heat transfer are affected by the severe property variations near the critical region with gravity. There is flow acceleration along the horizontal duct resulted from fluid density decrease due to the heat transfer from the wall and temperature variation is very steep near the top and vertical surfaces. Fluid properties variation becomes steeper as pressure approaches to the critical pressure. Buoyancy force variation with temperature becomes larger as pressure approaches to the critical point.

Local heat transfer coefficient distribution has large variation along the inner surface of the duct section. The heat transfer coefficient on the bottom surface is much bigger than those on the other two surfaces and it depends on the pressure in the duct. As pressure approaches to the critical pressure the heat transfer coefficient increases very rapidly. There is a peak of heat transfer coefficient distribution on the center of the bottom surface along the duct while there is not severe variation of the heat transfer coefficient on the top surface of the duct. With the increase of the pressure the location of the peak moves to downstream because of pseudocritical temperature increase. Nusselt number on the center of the bottom surface also has a peak where bulk fluid temperature is higher than the pseudocritical temperature and the peak decreases with the increase of pressure. Nusselt number variations along the duct are also compared with other correlations for various pressures in the duct. Its peak is much higher than what are predicted from previous heat transfer correlations, and the differences increase as pressure approaches to the critical pressure. This study analyzes the convective heat transfer characteristics in the horizontal duct with the effect of thermophysical properties variation near the critical region. Further experimental investigations are necessary for adequate prediction of the complicated heat transfer phenomena in the duct.

Acknowledgements

This study is supported by Wonkwang University in 2006. Technical assistance from Prism Co. is also appreciated.

References

[1] I.L. Pioro, H.F. Khartabil, R.B. Duffey, Heat transfer to supercritical fluids flowing in channels-empirical correlations (survey), Nucl. Eng. Des. 230 (2004) 69–91.
[2] A.J. Polyakov, Heat transfer under supercritical pressures, Adv. Heat Transfer 21 (1991) 1–50.
[3] W.B. Hall, Heat transfer near the critical point, Adv. Heat Transfer 7 (1971) 1–83.
[4] L.J. Li, C.X. Lin, M.A. Ebadian, Turbulent heat transfer to near-critical water in a heated curved pipe under the conditions of mixed convection, Int. J. Heat Mass Transfer 42 (16) (1999) 3147–3158.
[5] S.H. Lee, J.R. Howell, Turbulent developing convective heat transfer in a tube for fluids near the critical point, Int. J. Heat Mass Transfer 41 (10) (1998) 1205–1218.
[6] J.R. Howell, S.H. Lee, Convective heat transfer in the entrance region of a vertical tube for water near the thermodynamic critical point, Int. J. Heat Mass Transfer 42 (7) (1999) 1177–1187.
[7] E.S. Vlakhov, Z.L. Mieopol'skii, L.R. Khasanov-agaev, Heat transfer to a supercritical medium with mixed convection and rising flow in heated tubes, Teploenergetika 28 (11) (1981) 69–71.
[8] S. Koshizuka, N. Takano, Y. Oka, Numerical analysis of deterioration phenomena in heat transfer to supercritical water, Int. J. Heat Mass Transfer 38 (16) (1995) 3077–3084.
[9] V.A. Kurganov, A.G. Kaptilnyi, Flow structure and turbulent transport of a supercritical pressure fluid in a vertical heated tube under the conditions of mixed convection experimental data, Int. J. Heat Mass Transfer 36 (13) (1993) 3383–3392.
[10] S.M. Liao, T.S. Zhao, Measurements of heat transfer coefficients from supercritical carbon dioxide flowing in horizontal mini/micro channels, J. Heat Transfer 124 (2002) 413–420.
[11] S.M. Liao, T.S. Zhao, An experimental investigation of convection heat transfer to supercritical carbon dioxide in miniature tubes, Int. J. Heat Mass Transfer 45 (25) (2002) 5025–5034.
[12] C.H. Son, S.J. Park, An experimental study on heat transfer and pressure drop characteristics of carbon dioxide during gas cooling process in a horizontal tube, Int. J. Refrig. 29 (2006) 539–546.
[13] I.L. Pioro, R.B. Duffey, Experimental heat transfer in supercritical water flowing inside channels (survey), Nucl. Eng. Des. 235 (2005) 2407–2430.
[14] P. Asinari, Numerical prediction of turbulent convective heat transfer in mini/micro channels for carbon dioxide at supercritical pressure, Int. J. Heat Mass Transfer 48 (18) (2005) 3864–3879.
[15] J. Tatsumoto, K. Hata, K. Hama, Y. Shirai, M. Shiotsu, Numerical analysis of two-dimensional steady-state and transient heat transfer in a parallel duct filled with pressurized He II, Cryogenics 44 (2004) 273–283.
[16] D.M. McEligot, J.D. Jackson, Deterioration criteria for convective heat transfer in gas flow through non-circular ducts, Nucl. Eng. Des. 232 (2004) 327–333.
[17] M. Hirota, H. Fujita, H. Yokosawa, H. Itoh, Turbulent heat transfer in a square duct, Int. J. Heat Fluid Flow 18 (1997) 170–180.
[18] N. Yucel, R.T. Guven, Forced-convection cooling enhancement of heated elements in a parallel-plate channels using porous inserts, Numer. Heat Transfer, Part A 51 (3) (2007) 293–312.
[19] D.D. Luo, C.W. Leung, T.L. Chan, W.O. Wong, Flow and forced-convection characteristics of turbulent flow through parallel plates with periodic transverse ribs, Numer. Heat Transfer, Part A 48 (1) (2005) 43–58.
[20] B.M. Da Silva Miranda, N.K. Anand, Convective heat transfer in a channel with porous baffles, Numer. Heat Transfer, Part A 46 (5) (2004) 425–452.
[21] C.K.G. Lam, K. Bremhorst, A modified form of the k-model for predicting wall turbulence, J. Fluids Eng. 103 (1981) 456–460.
[22] H. Lester, S.G. John, S.K. George, Steam Tables, Hemisphere, New York, 1984.

[23] S.V. Patankar, Numerical Heat Transfer and Fluid Flow, Hemisphere, Washington, DC, 1980.
[24] S.S. Pitla, E.A. Groll, S. Ramadhyani, New Correlation for the Heat Transfer Coefficient During In-tube Cooling of Turbulent Supercritical Carbon dioxide, International Institute of Refrigeration Commissions B1, B2, E1 and E2, Purdue University Press, 2000, pp. 259–267.
[25] R.H. Hendricks, R.V. Simoneau, Survey of heat transfer to near critical fluids, NASA Technical Note, NASA TN D-5886, 1970.
[26] S.M. Liao, T.S. Zhao, A numerical investigation of laminar convection of supercritical carbon dioxide in vertical mini/micro tubes, Prog. Comput. Fluid Dyn. 2 (2/3/4) (2002) 144–152.
[27] N. Zhou, A. Krishnan, Laminar and turbulent heat transfer in flow of supercritical CO_2, in: 30th National Heat Transfer Conference, 1995, pp. 53–63.